INTERNATIONAL JOURNAL OF
NUMERICAL ANALYSIS AND MODELING
Volume 20, Number 6, Pages 870–895


**doi: 10.4208/ijnam2023-1038**

# HIGH-ORDER ENRICHED FINITE ELEMENT METHODS FOR ELLIPTIC INTERFACE PROBLEMS WITH DISCONTINUOUS SOLUTIONS

CHAMPIKE ATTANAYAKE, SO-HSIANG CHOU, AND QUANLING DENG

**Abstract.** Elliptic interface problems whose solutions are $C^0$ continuous have been well studied over the past two decades. The well-known numerical methods include the strongly stable generalized finite element method (SGFEM) and immersed FEM (IFEM). In this paper, we study numerically a larger class of elliptic interface problems where their solutions are discontinuous. A direct application of these existing methods fails immediately as the approximate solution is in a larger space that covers discontinuous functions. We propose a class of high-order enriched unfitted FEMs to solve these problems with implicit or Robin-type interface jump conditions. We design new enrichment functions that capture the imposed discontinuity of the solution while keeping the condition number from fast growth. A linear enriched method in 1D was recently developed using one enrichment function and we generalized it to an arbitrary degree using two simple discontinuous one-sided enrichment functions. The natural tensor product extension to the 2D case is demonstrated. Optimal order convergence in the $L^2$ and broken $H^1$-norms are established. We also establish superconvergence at all discretization nodes (including exact nodal values in special cases). Numerical examples are provided to confirm the theory. Finally, to prove the efficiency of the method for practical problems, the enriched linear, quadratic, and cubic elements are applied to a multi-layer wall model for drug-eluting stents in which zero-flux jump conditions and implicit concentration interface conditions are both present.

**Key words.** Generalized finite element method, elliptic interface, implicit interface jump condition, Robin interface jump condition, linear and quadratic finite elements.

## 1. Introduction

Consider the interface two-point boundary value problem

$$\begin{cases} -(\beta(x)u'(x))' + w(x)u(x) = f(x), \quad x \in (a,\alpha)\cup(\alpha,b), \\ u(a) = u(b) = 0, \end{cases} \tag{1}$$

where $w(x) \geq 0$, and $0 < \beta \in C[a,\alpha] \cup C[\alpha,b]$ is discontinuous across the interface $\alpha$ with the jump conditions on $u$ and its flux $q := -\beta u'$:

$$[u]_\alpha = \lambda F(q^+, q^-), \quad \lambda \in \mathbb{R},\ F : [c_1,d_1]^2 \to \mathbb{R}, \tag{2}$$

$$[\beta u']_\alpha = f_\alpha, \quad f_\alpha \in \mathbb{R}, \tag{3}$$

where the jump quantity

$$[s]_\alpha := s(\alpha^+) - s(\alpha^-), \quad s^\pm := s(\alpha^\pm) := \lim_{\epsilon\to 0^+} s(\alpha \pm \epsilon).$$

The primary variable $u$ may stand for the pressure, temperature, or concentration in a medium with certain physical properties and the derived quantity $q := -\beta u'$ is the corresponding Darcy velocity, heat flux, or concentration flux, which is equally important. The piecewise continuous $\beta$ reflects a nonuniform material or medium property (we do not require $\beta$ to be piecewise constant). The function $w(x)$ reflects the surroundings of the medium characterising the coefficient of the reaction term. The case of $\lambda = 0$ is widely studied, while the case of $\lambda > 0$ gives rise to a more

Received by the editors on February 25, 2022 and, accepted on October 2, 2023.
2000 *Mathematics Subject Classification.* 65N15, 65N30.

difficult situation. For example, the case of rightward concentration flow [29, 30, 31] imposes

$$\begin{cases} [u]_\alpha & = \lambda(\beta u')(\alpha^-) \\ [\beta u']_\alpha & = 0, \end{cases} \tag{4}$$

which generates an implicit condition since the left-sided derivative is unknown. Implicit interface conditions abound in higher dimensional applications [1, 16, 19, 21]. For definiteness, we will study a class of efficient enriched methods for problem (1) under the jump conditions (4),

The model problem (1), allowing the solution to be discontinuous at the interfaces, is a more general form of interface problem than the ones studied by Babuška *et. al.* using SGFEM [4, 3, 20] and by Li *et.al.* using immersed finite element method (IFEM) [22, 23, 25, 24]. In these works, the interface problem is assumed to have a continuous solution at the interfaces. For the case of the discontinuous solution at the interfaces, some IFE methods have also been developed, see for example [35, 36]. A large class of the methods is developed based on the unfitted meshes, which has been demonstrated to be more efficient than methods using fitted meshes, especially when the interface is moving [17]; see also [7, 10, 14, 15, 18, 29].

The generalized FEMs (GFEM) were first introduced to capture certain known features of the solution to the crack problem [5, 6, 13, 26]. However, it has been shown that GFEM suffers from a lack of robustness with respect to mesh configurations and bad conditioning. In general, the condition numbers of GFEM can grow with an order $\mathcal{O}(h^{-4})$ where $h$ characterizes the mesh size. This is two orders of magnitude worse than the standard FEM (known to be of order $\mathcal{O}(h^{-2})$). To resolve this issue, SGFEM has been developed [3, 4, 20] with an extra feature of robustness with respect to the mesh configurations. Further development of SGFEM has been active. For example, [34] extends the linear SGFEM to quadratic-order; [12] extends the method for eigenvalue interface problems, and [33] generalizes the SGFEM idea to isogeometric analysis with B-spline basis functions.

In 1D, when the solution to the underlying interface problem is continuous, a single enrichment function associated with the interface can be used for arbitrary high-order elements in the SGFEM. However, for an interface problem whose solution is discontinuous at interfaces, the natural extension with one enrichment function at each interface fails. A more sophisticated construction of enrichment functions is desired especially for high-order elements. This motivates the present work.

In our enriched FEM (might also call it as a GFEM), the approximation finite element space $V_h^{enr}$ takes the form:

$$V_h^{enr} := S_h + V_E = \{p_h + q_h\psi : \, p_h, q_h \in S_h, \psi \in F_{enr}\} \tag{5}$$

where $S_h$ is a standard finite element space (e.g., $\mathbb{P}_k$-conforming, $k \geq 1$),

$$V_E = \{q_h\psi : \, q_h \in S_h, \psi \in F_{enr}\}, \tag{6}$$

and the function $\psi$ is from the enrichment function space

$$F_{enr} := \text{span}\{\psi_0, \psi_1, \ldots, \psi_m\}, \ \dim(F_{enr}) = m + 1. \tag{7}$$

Here the basis functions $\psi_i$ capture the interface condition(s) at $\alpha$, e.g., zero or nonzero jump of the function value across $\alpha$. For example, for a continuous solution case, a single ($m = 0$) enrichment function suffices, whereas we show in this paper that for discontinuous solution case, we need two enrichment functions ($m = 1$) defined in (10). There are some distinct features about $V_h^{enr}$ in this case.

Firstly, the subspaces $S_h$ and $V_E$ have nonempty intersection, i.e., $S_h \cap V_E \neq \emptyset$. This nonempty intersection implies linear dependence on the set of functions that consist of the basis functions of $S_h$ and those of $V_E$. We show that the space $V_h^{enr}$ can be characterised by this set of functions when we remove the bubble basis functions associated with interfaces from $S_h$. Secondly, the local shape basis of IFEM utilizes information on discontinuous $\beta$ while GFEM does not. We propose an enriched method that does not require the discontinuous diffusion coefficient to be piecewise constant, which is an advantage. This difference affects the overhead and complexity of the convergence analysis. To carry out the error analysis in a conforming GFEM, we use the principle that the error in the finite element solution $u_h$ should be bounded by the approximation error in the finite element space $V_h^{enr}$:

$$||u - u_h|| \leq C \inf_{v \in V_h^{enr}} ||u - v||. \tag{8}$$

The optimal error estimate is established by demonstrating the existence of an optimal order approximate piecewise polynomial in $V_h^{enr}$. For the case with $C^0$ continuous solutions, this approximability was established by constructing an interpolating polynomial; see Deng and Calo [12] for details. With this in mind, the authors demonstrated the optimal convergence of GFEM solutions in *all* $\mathbb{P}_p-$conforming spaces ($p \geq 1$) enriched by the well-known hat-like enrichment function (cf. Eq. (71) below). On the other hand, Chou et. al. [11] used a single enrichment function to handle problem (1) with $[u]_\alpha \neq 0$ using the linear GFEM ($p = 1$). In this paper, we use two one-sided enrichment functions for each interface and show the effectiveness and convergence of the associated GFEM of all orders, i.e., $p \geq 1$. In addition to demonstrating optimal order convergence in the $L^2$ and broken $H^1$ norms, we also show superconvergence of nodal errors.

The organisation of the rest of the paper is as follows. In Section 2, we state the weak formulation for the implicit interface condition problem (1) with (4), and define enrichment functions and spaces. In Theorem 2.6, we show optimal order convergence in the $L^2$ and broken $H^1$ norms. Furthermore, in Theorem 2.7 we show $2p$ order convergence at the nodes and the exactness of the approximate solution at nodes for the piecewise constant diffusion case. Section 3 concerns its extension to a special case of 2D problems where the interface is a straight parallel (to a boundary) line. In Section 4, we provide numerical examples of a porous wall model to demonstrate the effectiveness of the present GFEM and confirm the convergence theory. Linear, quadratic, and cubic elements are tested. Furthermore, following the viewpoint of the SGFEM [3, 4, 12], we compare the condition numbers of our (discontinuous solution) method with those in the continuous solution case [2], and numerically show that they are comparable for the same mesh sizes. Finally, in Section 5 we give some concluding remarks.

## 2. Enrichment Functions and Spaces

**2.1. Weak Formulation.** Let $I^- = (a, \alpha)$,$I^+ = (\alpha, b)$, $I = (a, b)$, and define

$$H^1_{\alpha,0}(I) = \{v \in L^2(I) : v \in H^1(I^-) \cap H^1(I^+), v(a) = v(b) = 0\}.$$

We use conventional Sobolev norm notation. For example, $|u|_{1,J}$ denotes the usual $H^1$-seminorm for $u \in H^1(J)$, and $||u||^2_{i,I^-\cup I^+} = ||u||^2_{i,I^-} + ||u||^2_{i,I^+}, i = 1, 2$ for $u \in H^2_\alpha(I)$, where

$$H^2_\alpha(I) = H^2(I^-) \cap H^2(I^+).$$

The space $H^1_{\alpha,0}(I)$ is endowed with the $||\cdot||_{1,I^-\cup I^+}$ norm, and $H^2_\alpha(I)$ with the $||\cdot||_{2,I^-\cup I^+}$ norm. The higher-order spaces $H^m_\alpha(I)$ and $H^m_{\alpha,0}(I), m \geq 3$ are similarly

defined. With this in mind, the weak formulation of the problem (1) under (4) is: Given $f \in L^2(I)$, find $u \in H^1_{\alpha,0}(I)$ such that

$$a(u,v) = (f,v) \quad \forall v \in H^1_{\alpha,0}(I), \tag{9}$$

where

$$a(u,v) = \int_a^b \beta(x)u'(x)v'(x)dx + \int_a^b w(x)u(x)v(x)dx + \frac{[u]_\alpha[v]_\alpha}{\lambda},$$
$$(f,v) = \int_a^b f(x)v(x)dx.$$

The above weak formulation can be easily derived by integration-by-parts with (4). Since $\lambda > 0$, the bilinear form $a(\cdot,\cdot)$ is coercive and is bounded due to Poincaré inequality. By the Lax-Milgram theorem, a unique solution $u$ exists. Throughout the paper, we assume that the functions $\beta$, $f$, and $w$ are such that the solution $u \in H^p_\alpha(I), p \geq 2$.

**2.2. Enrichment Functions.** We now introduce an approximation space for the solution $u$. Let $a = x_0 < x_1 < \ldots < x_k < x_{k+1} < \ldots < x_N = b$ be a partition of $I$ and the interface point $\alpha \in (x_k, x_{k+1})$ for some $k$. As usual, the mesh size $h := \max_i h_i, h_i = x_{i+1} - x_i, i = 0, \ldots, N-1$. Define the two one-sided enrichment functions

$$\psi_0(x) := \begin{cases} 0 & x \in [a, x_k] \\ m_1(x - x_k) & x \in [x_k, \alpha) \\ 0 & x \in (\alpha, b] \end{cases} \text{ and } \psi_1(x) := \begin{cases} 0 & x \in [a, \alpha) \\ m_2(x - x_{k+1}) & x \in (\alpha, x_{k+1}] \\ 0 & x \in [x_{k+1}, b] \end{cases} \tag{10}$$

where

$$m_1 = \frac{1}{\alpha - x_k}, \quad m_2 = \frac{1}{\alpha - x_{k+1}}. \tag{11}$$

**Remark 2.1.**

- It is the enrichment function space $F_{enr} := \text{span}\{\psi_0, \psi_1\}$ that matters. Any two basis functions of $F_{enr}$ qualify, i.e., any pairs of nonzero $m_1$ and $m_2$ will guarantee convergence, as we shall show below. This space can also be spanned by one continuous and one one-sided function.

  For example, the familiar continuous

$$\tilde{\psi}_0(x) := \begin{cases} 0 & x \in [a, x_k] \\ \tilde{m}_1(x - x_k) & x \in [x_k, \alpha) \\ \tilde{m}_2(x - x_{k+1}) & x \in [\alpha, x_{k+1}] \\ 0 & x \in (\alpha, b] \end{cases} \text{ and a discontinuous } \quad \tilde{\psi}_1(x) := \psi_1(x) \tag{12}$$

  where

$$\tilde{m}_1 = \frac{\alpha - x_{k+1}}{x_{k+1} - x_k}, \quad \tilde{m}_2 = \frac{(\alpha - x_k)}{(x_{k+1} - x_k)}. \tag{13}$$

- We will adopt choice (11) since it makes the ensuing error analysis more transparent and simpler. It is simpler because as can be seen later that we can concentrate our error analysis separately on each subdomain for the symmetric pairs. If we use the unsymmetric ones, the order of estimates, of course, will stay the same, but the analysis details would be messy. Since

only the enrichment space matters, a good choice of basis simplifies the analysis.

- Note that the slopes $\tilde{m}_1, \tilde{m}_2$ in choice (13) are uniformly bounded by 1, while the slopes $m_1, m_2$ in choice (11) are not. We show in Appendix A that the bounded type may lead to a system of out-of-scale finite element equations while choice (11) does not. However, after a diagonal scaling, their resulting preconditioned systems have comparable condition numbers (cf. Section 4).

Let us describe the enriched space associated with $\psi_i, i = 0, 1$. Let $\bar{I} = \cup_0^{N-1} I_i, I_i = [x_i, x_{i+1}]$ and let $S_h^p$ be the standard $\mathbb{P}_p, p \geq 1$ conforming finite element space

$$S_h^p = \{v_h \in C(\bar{I}) : v_h|_{I_i} \in \mathbb{P}_p, i = 0, \ldots, N-1, v_h(a) = v_h(b) = 0\} \\ = \text{span}\{\phi_j, j \in \mathcal{N}_h^p\}, \tag{14}$$

where $\phi_i$'s are the Lagrange nodal basis functions of order $p$, and where the nodal index set $\mathcal{N}_h^p := \{1, 2, \cdots, pN-1\}$.

We denote the usual $\mathbb{P}_p$-interpolation operator by $\mathfrak{I}_h : C(\bar{I}) \to S_h^p$,

$$\mathfrak{I}_h^p g = \sum_{i=1}^{pN-1} g(t_i)\phi_i,$$

where $t_i, i \in \mathcal{N}_h^p$ are the nodes such that $\phi_i(t_j) = \delta_{ij}$. For each element $\tau = I_i$, the local interpolation operator $\mathfrak{I}_\tau^p$ is

$$\mathfrak{I}_\tau^p g := \mathfrak{I}_h^p g\Big|_\tau = \sum_{j \in \mathcal{N}_\tau^p} g(t_j)\phi_j, \tag{15}$$

and $\mathcal{N}_\tau^p \subset \mathcal{N}_h^p$ is the set of nodes associated with $\tau$. Define the enriched finite element space

$$\overline{S}_h^p = S_h^p + S_{h,E} = \{v_h + w_h, v_h \in S_h^p, w_h \in S_{h,E}\} \tag{16}$$

and

$$S_{h,E} := \{w_h : w_h = v\psi_0 + w\psi_1,\, v, w, \in S_h^p\}.$$

It will be shown later that algebraic sum '+' in (16) cannot be a direct sum '$\oplus$' since the intersection space, $S_h^p \cap S_{h,E}$, is not empty.

The GFEM for problem (1) under (4) is to find $u_h \in \overline{S}_h^p \subset H_{\alpha,0}^1$ such that

$$a(u_h, v_h) = (f, v_h) \quad \forall v_h \in \overline{S}_h^p. \tag{17}$$

To derive the corresponding linear algebraic system of equations, we need to form a basis for the enriched space $\overline{S}_h^p$, which we characterize as below.

**2.3. Structure of the enrichment finite element space.** It suffices to analyze the structure of the enriched space restricted to the interface element $[x_k, x_{k+1}]$. To this end, we first concentrate on the reference element $[0, 1]$ with an interface point $\hat{\alpha}$. Let $\xi_i = i/p, i = 0, \ldots, p$, be the evenly distributed nodes and let the corresponding Lagrange interpolating polynomials be

$$q_i(x) = \prod_{j \neq i} \frac{(x - \xi_j)}{(\xi_i - \xi_j)}.$$

The local enriched space is

$$V_{h,loc}^{enr} := V_{loc} + V_E := \text{span}\{q_0, q_1, \ldots, q_{p-1}, q_p\} + \text{span}\{q_i\psi_0, q_i\psi_1\}_{i=0}^p. \tag{18}$$

For $p \geq 2$, we will refer to the $p-1$ functions $\{q_i\}_{i=1}^{p-1}$ as the bubble functions since they vanish at the endpoints. Note that $q_0(0) = 1$ and $q_p(1) = 1$. We will show in Lemma 2.2 that the bubble functions belong to $V_E$, and consequently

$$\dim(V_{h,loc}^{enr}) = \dim(V_{loc} + V_E) = 2 + 2(p+1).$$

**Remark 2.1.** *Note that there is no bubble function for the linear case ($p = 1$). Moreover, there holds $V_{loc} \cap V_E = \emptyset$. Thus, $V_{h,loc}^{enr} := V_{loc} \oplus V_E$ and the dimension is $dim(V_{h,loc}^{enr}) = dim(V_{loc} + V_E) = 2 + 2(p+1) = 6$.*

**Lemma 2.2 (Local linear dependence).** *Let $p \geq 2$. For any bubble function $q_i, 1 \leq i \leq p-1$, we have*

$$q_i \in V_E := span\{q_k\psi_0, q_k\psi_1\}_{k=0}^{p}, \tag{19}$$

*i.e., there exist $s_{ikj}, 0 \leq k \leq p, j = 0, 1$, such that*

$$q_i = \sum_{j=0}^{1}\sum_{k=0}^{p} s_{ikj} q_k \psi_j.$$

*Proof.* We only prove the theorem for $p = 2$ since the proof for general $p$ follows closely in this case but with more complicated indices. Note that there is only one bubble function $q_1$ for $p = 2$. On $[0, \hat{\alpha}]$, $\psi_1 = 0$ and we need to show the existence of $s_{1k0}$ such that $q_1 = \sum_{k=0}^{2} s_{1k0}\psi_0 q_k$. Since $m_1$ can be absorbed into $s_{1k0}$, we can assume $m_1 = 1$ in the following calculation so that $\psi_0 = x$. Expressing $q_k$ as a Taylor polynomial

$$q_k = q_k(0) + q_k'(0)x + \frac{q_k''(0)}{2}x^2$$

and comparing the coefficients of $x, x^2, x^3$ of

$$q_1(0) + q_1'(0)x + q_1''(0)x^2 = \sum_{k=0}^{2} s_{1k0}\left(q_k(0)x + q_k'(0)x^2 + \frac{q_k''(0)}{2}x^3\right) \tag{20}$$

we have

$$\sum_{k=0}^{2} s_{1k0} q_k(0) = q_1'(0), \tag{21}$$

$$\sum_{k=0}^{2} s_{1k0} q_k'(0) = q_1''(0), \tag{22}$$

$$\sum_{k=0}^{2} s_{1k0} q_k''(0) = 0, \tag{23}$$

whose coefficient matrix is the Wronskian matrix evaluated at $x = 0$

$$\begin{pmatrix} q_0(0) & q_1(0) & q_2(0) \\ q_0'(0) & q_1'(0) & q_2'(0) \\ q_0''(0) & q_1''(0) & q_2''(0) \end{pmatrix}. \tag{24}$$

Since the Wronskian is nonsingular, $s_{100}, s_{110}, s_{120}$ exist. Similarly for $[\hat{\alpha}, 1]$, we use the Taylor polynomials at $x = 1$. All the equations are the same except they are evaluated at $x = 1$. Thus $s_{101}, s_{111}, s_{121}$ exist. For the general case, the matrix in (24) is a Wronskian matrix of order $p$. □

The approximability of $V_{h,loc}^{enr}$-functions on the reference element is given below

**Theorem 2.3** (Local approximation)**.** *Let $\chi_i, i = 1, 2$ be the characteristic functions of $[0, \hat{\alpha}]$ and $[\hat{\alpha}, 1]$, respectively. Define the space*

$$W = \{w : w = w_1\chi_1 + w_2\chi_2, w_i \in \mathbb{P}_p, i = 1, 2\}. \tag{25}$$

*Then*

$$W \subset V_{h,loc}^{enr}.$$

*In other words, given two polynomials*

$$u_1 = \sum_{l=0}^{p} a_l x^l \text{ and } \quad u_2 = \sum_{l=0}^{p} b_l (x-1)^l,$$

*there exist unique $\zeta_0, \zeta_p; \{\zeta_i\}_{i=p+1}^{2p+1}, \{\zeta_j\}_{j=2p+2}^{3p+2}$ such that*

$$\sum_{i=1}^{2} \chi_i u_i = \sum_{j=0,p} \zeta_j q_j + \sum_{j=0}^{p} \zeta_{j+p+1} q_j \psi_0 + \sum_{j=0}^{p} \zeta_{j+2p+2} q_j \psi_1. \tag{26}$$

*Proof.* To prove the uniqueness of the solution of the square system in the unknown $\zeta_i$'s, we proceed as follows:

$$\sum_{i=0,p} \zeta_i q_i + \sum_{i=0}^{p} \zeta_{i+(p+1)} q_i \psi_0 = \sum_{l=0}^{p} a_l x^l, \tag{27}$$

$$\sum_{i=0,p} \zeta_i q_i + \sum_{i=0}^{p} \zeta_{i+2(p+1)} q_i \psi_1 = \sum_{l=0}^{p} b_l (x-1)^l. \tag{28}$$

We can take $m_1 = m_2 = 1$ because they can be absorbed into coefficients. Switching the indices in

$$\sum_{i=0,p} \zeta_i \left( \sum_{l=0}^{p} \frac{q_i^{(l)}(0)}{l!} x^l \right) + \sum_{i=0}^{p} \zeta_{i+(p+1)} \left( \sum_{l=0}^{p} \frac{q_i^{(l)}(0)}{l!} x^l \right) x = \sum_{l=0}^{p} a_l x^l,$$

we obtain

$$\sum_{l=0}^{p} \left( \sum_{i=0,p} \zeta_i \frac{q_i^{(l)}(0)}{l!} \right) x^l + \sum_{l=1}^{p+1} \left( \sum_{i=0}^{p} \zeta_{i+(p+1)} \frac{q_i^{(l-1)}(0)}{(l-1)!} \right) x^l = \sum_{l=0}^{p} a_i x^l. \tag{29}$$

Similarly from

$$\sum_{i=0,p} \zeta_i \left( \sum_{l=0}^{p} \frac{q_i^{(l)}(1)}{l!} (x-1)^l \right) + \sum_{i=0}^{p} \zeta_{i+2(p+1)} \left( \sum_{l=0}^{p} \frac{q_i^{(l)}(1)}{l!} (x-1)^l \right) (x-1)$$
$$= \sum_{l=0}^{p} b_l (x-1)^l,$$

we have

$$\sum_{l=0}^{p} \left( \sum_{i=0,p} \zeta_i \frac{q_i^{(l)}(1)}{l!} \right) (x-1)^l + \sum_{l=1}^{p+1} \left( \sum_{i=0}^{p} \zeta_{i+2(p+1)} \frac{q_i^{(l-1)}(1)}{(l-1)!} \right) (x-1)^l \tag{30}$$
$$= \sum_{l=0}^{p} b_l (x-1)^l.$$

Comparing the coefficients of $x^{p+1}$ from the two sides of (29) and (30), we see that

$$\sum_{i=0}^{p} \zeta_{i+(p+1)} q_i^{(p)}(0) = 0, \tag{31}$$

$$\sum_{i=0}^{p} \zeta_{i+2(p+1)} q_i^{(p)}(1) = 0. \tag{32}$$

Comparing the coefficients of $x^l, 0 \le l \le p$, we arrive at

$$\sum_{i=0,p} \zeta_i \frac{q_i^{(l)}(0)}{l!} + \sum_{i=0}^{p} \zeta_{i+(p+1)} \frac{q_i^{(l-1)}(0)}{(l-1)!} = a_l,$$

$$\sum_{i=0,p} \zeta_i \frac{q_i^{(l)}(1)}{l!} + \sum_{i=0}^{p} \zeta_{i+2(p+1)} \frac{q_i^{(l-1)}(1)}{(l-1)!} = b_l,$$

with the understanding that the second terms on the left drop out when $l = 0$. Collecting terms, we see that the square system is

$$\sum_{i=0}^{p} \zeta_{i+(p+1)} q_i^{(p)}(0) = 0, \tag{33}$$

$$\sum_{i=0,p} \zeta_i \frac{q_i^{(l)}(0)}{l!} + \sum_{i=0}^{p} \zeta_{i+(p+1)} \frac{q_i^{(l-1)}(0)}{(l-1)!} = a_l,\ 0 \le l \le p, \tag{34}$$

$$\sum_{i=0}^{p} \zeta_{i+2(p+1)} q_i^{(p)}(1) = 0, \tag{35}$$

$$\sum_{i=0,p} \zeta_i \frac{q_i^{(l)}(1)}{l!} + \sum_{i=0}^{p} \zeta_{i+2(p+1)} \frac{q_i^{(l-1)}(1)}{(l-1)!} = b_l,\ 0 \le l \le p. \tag{36}$$

Since this system is square it suffices to show that all $\zeta_i$'s are zero when $a_l = b_l = 0 \le l \le p$. First, observe that $\zeta_0 = \zeta_p = 0$. In fact, with $l = 0$ using the second and fourth equations we have

$$\zeta_0 q_0(0) + \zeta_p q_p(0) = 0,$$
$$\zeta_0 q_0(1) + \zeta_p q_p(1) = 0.$$

The conclusion follows using $q_p(1) = 1, q_p(0) = 0, q_0(0) = 1, q_0(1) = 0$. As a consequence, (34) and (36) decouple and simplify to two linear systems

$$\sum_{i=0}^{p} \zeta_{i+(p+1)} q_i^{(l-1)}(0) = 0, \tag{37}$$

$$\sum_{i=0}^{p} \zeta_{i+2(p+1)} q_i^{(l-1)}(1) = 0 \tag{38}$$

whose coefficient matrices are nonsingular, being Wronskian matrices. Thus, all $\zeta_i = 0$. □

Transforming the above results on [0,1] to $[x_k, x_{k+1}]$, we have the following result.

**Lemma 2.4** (Local interpolant)**.** *Let $g \in C(\bar{\omega}), \omega = (c, d)$ and $I^p_{h,\omega} g \in \mathbb{P}_p$ be the interpolating polynomial of $g$ at $p+1$ nodes $\xi_i = c + i[d-c]/p, i = 0, \ldots, p$. Then*

*for* $v \in C[x_k, \alpha] \cap C[\alpha, x_{k+1}]$*, there exists a* $\rho \in V_h^{enr}\Big|_{[x_k, x_{k+1}]}$ *such that*

$$\left(I^p_{h,[x_k,\alpha]} v\right) \chi_{[x_k,\alpha]} + \left(I^p_{h,[\alpha,x_{k+1}]} v\right) \chi_{[\alpha,x_{k+1}]} = \rho. \tag{39}$$

Combining the classical results for non-interface elements and Lemma 2.4 for the interface element, we have

**Lemma 2.5** (Global interpolant)**.** *Define a global interpolant* $\mathfrak{I}_{h,E} : C[a, \alpha] \cap C([\alpha, b]) \to \mathbb{R}$ *by* $\mathfrak{I}_{h,E} v = I^p_{h,\omega} v, \omega = [x_k, \alpha], [\alpha, x_{k+1}], [x_i, x_{i+1}], i = 0, \ldots, k-1, k+1, \ldots, N-1$*. Then*

$$|v - \mathfrak{I}_{h,E} v|_{1, I^- \cup I^+} \leq C h^p |v|_{p+1, I^- \cup I^+}.$$

**Theorem 2.6** (Error Estimate)**.** *Let* $u$ *be the exact solution and* $u_h$ *be the approximate solution of (9) and (17), respectively. Then there exists a constant* $C > 0$ *such that*

$$\|u - u_h\|_{0, I^- \cup I^+} + h \|u - u_h\|_{1, I^- \cup I^+} \leq C h^{p+1} \|u\|_{p+1, I^- \cup I^+} \tag{40}$$

*provided that the norm of the exact solution on the right side is finite. The constant* $C$ *is independent of* $h$ *and* $\alpha$ *but depends on the ratio* $\rho := \frac{\beta^*}{\beta_*}$ *with* $\beta^* = \sup_{x \in [a,b]} \beta(x)$ *and* $\beta_* = \inf_{x \in [a,b]} \beta(x)$*.*

*Proof.* Subtracting (9) from (17), we have

$$a(u - u_h, q_h) = 0 \quad \forall q_h \in \overline{S}_h.$$

Using the boundedness and coercivity properties of the bilinear form $a(\cdot, \cdot)$, we get

$$\begin{aligned} \beta_* |u - u_h|^2_{1,I} &\leq a(u - u_h, u - u_h) = a(u - u_h, u - q_h) \\ &\leq \beta^* |u - u_h|_{1,I} |u - q_h|_{1,I}, \end{aligned}$$

where $\beta^* = \sup_{x \in [a,b]} \beta(x)$ and $\beta_* = \inf_{x \in [a,b]} \beta(x)$. Thus, by Cea's lemma and Lemma 2.5

$$\begin{aligned} |u - u_h|_{1,I} &\leq \frac{\beta^*}{\beta_*} \inf |u - q_h|_{1,I} \\ &\leq \frac{\beta^*}{\beta_*} |u - \mathfrak{I}_{h,E} u|_{1,I} \\ &\leq C h^p \|u\|_{p+1, I^- \cup I^+}. \end{aligned}$$

Then the usual duality argument leads to

$$\|u - u_h\|_{0,I} \leq C h^{p+1} \|u\|_{p+1, I^- \cup I^+}.$$

□

We note that the jump ratios $\rho := \frac{\beta^*}{\beta_*}$ are of moderate size for the wall model in Section 4.

**Theorem 2.7** ($2p$**-th order accuracy at nodes).** *Suppose that* $\beta \in C^{p+1}(a, \alpha) \cap C^{p+1}(\alpha, b), p \geq 1$ *and* $w(x) = 0$*. Let* $u$ *be the exact solution and* $u_h$ *be the approximate solution of (9) and (17), respectively. Then there exists a constant* $C > 0$ *such that*

$$|u(\xi) - u_h(\xi)| \leq C h^{2p} ||u||_{p+1, I^- \cup I^+}, \quad \xi = x_i, 1 \leq i \leq n-1, \tag{41}$$

*where $C$ depends on certain norms of Green's function at $\xi$.*

**Superconvergence**. *Furthermore, if $\beta$ is piecewise constant with respect to $[a,\alpha]$ and $[\alpha,b]$, then*

$$u(\xi) = u_h(\xi) \quad \forall \xi = x_i, 1 \le i \le n-1. \tag{42}$$

*Proof.* Let $g = G(\cdot,\xi), \xi \neq \alpha$ be the Green's function satisfying

$$a(G(\cdot,\xi), v) =< \delta(x-\xi), v >, \quad v \in H^1_{0,\alpha}(a,b)$$

whose existence is guaranteed by the Lax-Milgram theorem, since in 1D point evaluation is a bounded operator. We can find Green's function via the classical formulation (for simplicity let $[a,b] = [0,1]$ and $\xi < \alpha$):

$$\begin{aligned} -(\beta g')' &= \delta(x-\xi), 0 < x < 1, & g(0) &= g(1) = 0, \\ [g]_\alpha &= \gamma [g']_\alpha, & [\beta g']_\alpha &= 0, \\ [g]_\xi &= 0, & [\beta g']_\xi &= 1. \end{aligned}$$

Define

$$K(x) := \int_0^x \frac{1}{\beta(t)} dt,\ 0 \le x \le \alpha; \quad K^c(x) := \int_x^1 \frac{1}{\beta(t)} dt,\ \alpha \le x \le 1. \tag{43}$$

Then, similar to the techniques in [10] we have

$$G(x,\xi) = \begin{cases} c_1 K(x), & 0 \le x \le \xi \\ c_3(K(x) - K(\xi)) + c_1 K(\xi), & \xi \le x < \alpha \\ -c_2 K^c(x), & \alpha < x \le 1, \end{cases} \tag{44}$$

where with $\gamma = \frac{\lambda \beta^+ \beta^-}{(\beta^- - \beta^+)}$, $c_3 = \dfrac{K(\xi)}{-K^c(\alpha) - K(\alpha) - \lambda}$, $c_2 = c_3$, $c_1 = 1 + c_3$.

Thus, for $\xi < \alpha$, $g = G(\cdot,\xi) \in H^{p+1}(\Omega)$, for $\Omega = (a,\xi), (\xi, x_k), (x_k, \alpha), (\alpha, x_{k+1})$, and $(x_{k+1}, b)$. Similar regularity holds if $\xi > \alpha$. Using the local estimates in Lemma 2.5, we conclude that that there exists $I_h g \in \bar{S}_h^p$ such that

$$|g - I_h g|_{1,\Omega} \le C h^p ||g^{(p+1)}||_{0,\Omega} \tag{45}$$

for all the $\Omega$'s listed above. Now with $\xi = x_i$

$$e(x_i) = a(g,e) = a(g - I_h g, e)$$

implies that

$$\begin{aligned} |e(x_i)| &\le C h^p ||g||_{p+1,*}\, h^p ||u||_{p+1, I^- \cup I^+} \\ &\le C h^{2p} ||g||_{p+1,*} ||u||_{p+1, I^- \cup I^+} \end{aligned}$$

where $||g||^2_{p+1,*} := \sum ||g||^2_{p+1,\Omega}$, the summation being over all the $\Omega$'s listed above.

We next prove the assertion (42). Since $\beta$ is piecewise constant, Green's function (44) is piecewise linear in $x$ with fixed $\xi_i = x_i, 1 \le i \le n-1$. Hence, $g = G(\cdot, x_i)$ is in $\bar{S}_h^p$ by Theorem 2.3 and consequently

$$e(x_i) = a(g,e) = 0.$$

□

Let us point out in passing that the assertion (41) still holds if $0 \le w \in C^p[a,b]$, which can be proven by the techniques of the reduction theorem (p. 4, [28]) to the divergence form. Studies on the superconvergence of other numerical methods for interface problems such as the IFEM or 1-D immersed finite volume methods can be found in [8, 9]. It seems very promising that one can develop a parallel

superconvergence theory to the one in [8] for our high-order enriched finite elements. We are currently investigating this possibility.

We will use the preconditioned conjugate gradient method to solve the resulting finite element equation. The matrix $D_A$, the diagonal part of $A$, is used as a preconditioner, and we solve iteratively a system of the form $D_A^{-1/2}AD_A^{-1/2}y = b$. The scaled condition number $\kappa_2(D_A^{-1}A)$ (SCN)[4] for the higher order method will be computed in Section 4.

## 3. Extension to Two Dimensions

Let $\Omega := [a,b] \times [c,d]$ be a rectangular domain with a vertical or horizontal interface $\Gamma := \{(x,y) : x = \alpha\} \cap \bar{\Omega}$ or $\Gamma := \{(x,y) : y = \alpha\} \cap \bar{\Omega}$ that separates the domain into two subdomains $\Omega^-$ and $\Omega^+$. Then, $\Gamma = \bar{\Omega}^- \cap \bar{\Omega}^+$ with $\Omega^- \cap \Omega^+ = \emptyset$ and $\bar{\Omega}^- \cup \bar{\Omega}^+ = \bar{\Omega}$. We now consider the following interface elliptic problem: Find $u : \bar{\Omega} \to \mathbb{R}$ such that

$$\begin{cases} -\nabla \cdot (\beta(\mathbf{x})\nabla u) + w(\mathbf{x})u(\mathbf{x}) = f(\mathbf{x}), & \mathbf{x} \in \Omega \backslash \Gamma, \\ u(\mathbf{x}) = 0, & \mathbf{x} \in \partial\Omega, \end{cases} \tag{46}$$

where $w(\mathbf{x}) \geq 0$, and $0 < \beta \in C(\bar{\Omega}^-) \cup C(\bar{\Omega}^+)$ is discontinuous across the interface $\Gamma$. As in 1D, we impose the 2D jump conditions on $u$ and its flux $q := -\beta\nabla u$ across $\Gamma$:

$$\begin{cases} [u]_\alpha & = \lambda(\beta\nabla u \cdot \mathbf{n})(\alpha^-), \\ [\beta\nabla u \cdot \mathbf{n}]_\alpha & = 0, \end{cases} \tag{47}$$

where the jump quantity $[\cdot]$ is understood similarly. We consider this interface problem to demonstrate our method for simplicity. Essentially, this work generalizes the SGFEM developed in [4, 20] for the straight interface problem (46)-(47) with $\lambda = 0$ to the case with $\lambda \neq 0$.

### 3.1. Enrichment Functions and Weak Formulation in 2D.

Define

$$H^1_{\alpha,0}(\Omega) = \{v \in L^2(\Omega) : v \in H^1(\Omega^-) \cap H^1(\Omega^+), v = 0 \text{ on } \partial\Omega\}.$$

We use conventional Sobolev norm notation. For example, $|u|_{1,J}$ denotes the usual $H^1$-seminorm for $u \in H^1(J)$, and $||u||^2_{i,\Omega^- \cup \Omega^+} = ||u||^2_{i,\Omega^-} + ||u||^2_{i,\Omega^+}, i = 1,2$ for $u \in H^2_\alpha(\Omega)$, where

$$H^2_\alpha(\Omega) = H^2(\Omega^-) \cap H^2(\Omega^+).$$

The space $H^1_{\alpha,0}(\Omega)$ is endowed with the $||\cdot||_{1,\Omega^- \cup \Omega^+}$ norm, and $H^2_\alpha(\Omega)$ with the $||\cdot||_{2,\Omega^- \cup \Omega^+}$ norm. The higher-order spaces $H^m_\alpha(\Omega)$ and $H^m_{\alpha,0}(\Omega), m \geq 3$ are similarly defined. With this in mind, the weak formulation of the problem (46) under (47) is: Given $f \in L^2(\Omega)$, find $u \in H^1_{\alpha,0}(\Omega)$ such that

$$a(u,v) = (f,v) \quad \forall v \in H^1_{\alpha,0}(\Omega), \tag{48}$$

where

$$a(u,v) = \int_\Omega \beta(\mathbf{x})\nabla u(\mathbf{x}) \cdot \nabla v(\mathbf{x}) d\mathbf{x} + \int_\Omega w(\mathbf{x})u(\mathbf{x})v(\mathbf{x})d\mathbf{x} + \frac{1}{\lambda}\int_\Gamma [u]_\alpha [v]_\alpha d\sigma,$$

$$(f,v) = \int_\Omega f(\mathbf{x})v(\mathbf{x})d\mathbf{x}.$$

As in 1D, the above weak formulation can be easily derived by integration-by-parts with (47). With $\lambda > 0$, the bilinear form $a(\cdot,\cdot)$ is coercive due to Poincaré inequality (when $w = 0$ ) and is bounded. By the Lax-Milgram theorem, a unique

solution $u$ exists. Throughout the paper, we assume that the functions $\beta$, $f$, and $w$ are such that the solution $u \in H^p_\alpha(\Omega), p \geq 2$.

We assume from now on that the interface is $x = \alpha$ and define a regular rectangular mesh on $\Omega$ as follows. Let $a = x_0 < x_1 < \ldots < x_k < x_{k+1} < \ldots < x_N = b$ be a partition of $I = (a, b)$ with $\alpha \in (x_k, x_{k+1})$ for some $k$. Similarly, let $c = y_0 < y_1 < \ldots < y_M = b$ be a partition of $J = (c, d)$. Let

$$I_i = [x_i, x_{i+1}],\ J_j = [y_j, y_{j+1}],\ R_{i,j} = I_i \times J_j, \quad 0 \leq i \leq N_x - 1, 0 \leq j \leq N_y - 1$$

then $R_{i,j}$ is an element and $R_h = \{R_{i,j}\}$ is the rectangular mesh for $\Omega$. For each $R = R_{i,j}$, we let $h(R) = \max\{h_1, h_2\}, \rho(R) = \min\{h_1, h_2\}$ where $h_1 = |x_i - x_{i+1}|, h_2 = |y_j - y_{j+1}|$. We assume $R_h$ is regular, i.e., there exists a constant $C > 0$ such that

$$\max_{R \in R_h} \frac{h(R)}{\rho(R)} \leq C.$$

Furthermore, the intersection of the interface $x = \alpha$ with the interface element boundary $\partial R_i$ cannot be a vertex or have nonzero length.

Recall from (14) that $S_h$ is the standard $\mathbb{P}_p, p \geq 1$ conforming finite element space on $I$. Similarly, we define the standard $\mathbb{P}_p, p \geq 1$ conforming finite element space on $J$

$$\begin{aligned} \mathcal{S}^p_h &= \{v_h \in C(\bar{J}) : w_h|_{J_i} \in \mathbb{P}_p, i = 0, \ldots, N_y - 1, w_h(c) = w_h(d) = 0\} \\ &= \text{span}\{\chi_j, j \in \mathcal{M}^p_h\}, \end{aligned} \tag{49}$$

where $\chi_i$'s are the Lagrange nodal basis functions of order $p$ with the nodal index set $\mathcal{M}^p_h := \{1, 2, \cdots, pN_y - 1\}$.

It is then natural to define the 2D enriched finite element space $\mathcal{E}^p_h$ as the tensor product of the 1D enriched space $\overline{S}^p_h$ of (16) and $\mathcal{S}^p_h$, the 1D conforming space of (49) in the $y-$direction:

$$\mathcal{E}^p_h = \overline{S}^p_h \otimes \mathcal{S}^p_h. \tag{50}$$

The GFEM or the enriched FEM for problem (46) under (47) is to find $u_h \in \mathcal{E}^p_h \subset H^1_{\alpha,0}(\Omega)$ such that

$$a(u_h, v_h) = (f, v_h) \quad \forall v_h \in \mathcal{E}^p_h. \tag{51}$$

The bilinear form $a(\cdot, \cdot)$ has three parts. When $\beta|_{\Omega^-}, \beta|_{\Omega^+}, w|_{\Omega^+}$ and $w|_{\Omega^+}$ are constant, one can derive the 2D matrices as tensor-products of 1D matrices. With this in mind, for two basis functions $\phi^p_{i_x}(x)\phi^p_{i_y}(y), \phi^p_{j_x}(x)\phi^p_{j_y}(y) \in \mathcal{E}^p_h$, the matrix entries are

$$(w\phi^p_{i_x}(x)\phi^p_{i_y}(y), \phi^p_{j_x}(x)\phi^p_{j_y}(y)) = (w\phi^p_{i_x}(x), \phi^p_{j_x}(x)) \cdot (\phi^p_{i_y}(y), \phi^p_{j_y}(y)), \tag{52}$$

where

$$\begin{aligned} (w\phi^p_{i_x}(x), \phi^p_{j_x}(x)) &= \int_a^b w\phi^p_{i_x}(x)\phi^p_{j_x}(x)\ \mathrm{d}x, \\ (\phi^p_{i_y}(y), \phi^p_{j_y}(y)) &= \int_c^d \phi^p_{i_y}(y)\phi^p_{j_y}(y)\ \mathrm{d}y. \end{aligned} \tag{53}$$

Similarly,

(54)
$$\begin{aligned}(\beta\nabla\phi^p_{i_x}(x)\phi^p_{i_y}(y), \nabla\phi^p_{j_x}(x)\phi^p_{j_y}(y)) &= (\beta\partial_x\phi^p_{i_x}(x), \partial_x\phi^p_{j_x}(x)) \cdot (\phi^p_{i_y}(y), \phi^p_{j_y}(y)),\\ &\quad + (\beta\phi^p_{i_x}(x), \phi^p_{j_x}(x)) \cdot (\partial_y\phi^p_{i_y}(y), \partial_y\phi^p_{j_y}(y)),\\ \int_\Gamma [\phi^p_{i_x}(x)\phi^p_{i_y}(y)]_\alpha [\phi^p_{j_x}(x)\phi^p_{j_y}(y)]_\alpha d\sigma &= \int_c^d [\phi^p_{i_x}(x)\phi^p_{i_y}(y)]_\alpha [\phi^p_{j_x}(x)\phi^p_{j_y}(y)]_\alpha dy\\ &= ([\phi^p_{i_x}(x)]_\alpha, [\phi^p_{j_x}(x)]_\alpha) \cdot (\phi^p_{i_y}(y), \phi^p_{j_y}(y)).\end{aligned}$$

where $([\phi^p_{i_x}(x)]_\alpha, [\phi^p_{j_x}(x)]_\alpha) = [\phi^p_{i_x}(x)]_\alpha \cdot [\phi^p_{j_x}(x)]_\alpha$.

Using this property of the discretization, the GFEM (51) leads to the matrix problem of the form

$$(K_{x,\beta} \otimes M_y + M_{x,\beta} \otimes K_y)U + (M_{x,w} \otimes M_y)U + (J_{x,\lambda} \otimes M_y)U = F, \tag{55}$$

where the 1D matrices can be constructed from the inner products above and where $U \in \mathbb{R}^{(p(N_x+1)+2)\cdot(pN_y-1)}$ is a stack of column vectors $U_{i,y} \in \mathbb{R}^{pN_y-1}, 1 \le i \le p(N_x+1)+2$.

**3.2. The approximability of the enriched space.** Let $\hat{R} = [0,1] \times [0,1]$ be the reference element of the tensor mesh of $\Omega = \cup_k R_k$, i.e, there exists a *unique* bijective affine transformation $F_k$ such that $F_k(\hat{R}) = R_k$ for every $k$. The interface $x = \hat{\alpha}$ separates $\hat{R}$ into $\hat{R}^+$ and $\hat{R}^-$. Then the 2D counterpart of Theorem 2.3 still holds.

**Theorem 3.1** (Local approximation)**.** *Let $\chi_i, i = 1,2$ be the characteristic functions of $\hat{R}^-$ and $\hat{R}^+$, respectively. Define the space*

$$W = \{w : w = w_1\chi_1 + w_2\chi_2, w_i \in \mathbb{Q}_p := \mathbb{P}_p \otimes \mathbb{P}_p, i = 1,2\}. \tag{56}$$

*Then*

$$W \subset \mathcal{V}^{enr}_{h,loc},$$

*where $\mathcal{V}^{enr}_{h,loc}$ is the local enriched space, $\mathcal{V}^{enr}_{h,loc} = F_k^{-1}(\mathcal{E}^p_h|_{R^k})$.*

*Proof.* First note that each $F_k^{-1}$ sends the interface $x = \alpha$ in an interface element $R_k$ to an interface $\hat{x} = \hat{\alpha}$ in $\hat{R}$. It suffices to consider $w_i$ having the special form of basis functions

$$w_i(x,y) = X_i(x)Y_i(y), X_i, Y_i \in \mathbb{P}_p, i = 1,2.$$

Then using Theorem 2.3 to conclude $X_i$ belongs to the $\bar{S}^p_h$-space on $[0,1]$ and the fact that $F_k^{-1}$ preserves the tensor product structure of (50) complete the proof. □

Using the above theorem, it is not hard to see that the 2D version of Lemma 2.4 and Lemma 2.5 holds respectively due to the optimal order of approximation of $\mathbb{Q}_p(\hat{R})$ to $H^2(\hat{R})$ functions under the regular mesh assumption. Consequently, the 2D version of Theorem 2.6 holds and we have

**Theorem 3.2** (Error estimate)**.** *Let $u$ be the exact solution and $u_h$ be the approximate solution of (48) and (51), respectively. Then there exists a constant $C > 0$ such that*

$$\|u - u_h\|_{0,\Omega^-\cup\Omega^+} + h\|u - u_h\|_{1,\Omega^-\cup\Omega^+} \le Ch^{p+1}\|u\|_{p+1,\Omega^-\cup\Omega^+} \tag{57}$$

*provided that the norm of the exact solution on the right side is finite. The constant $C$ is independent of $h$ and $\alpha$ but depends on the ratio $\rho := \frac{\beta^*}{\beta_*}$ with $\beta^* = \sup_{\mathbf{x}\in\bar{\Omega}} \beta(\mathbf{x})$ and $\beta_* = \inf_{\mathbf{x}\in\bar{\Omega}} \beta(\mathbf{x})$.*

## 4. Numerical Experiments

In this section, we present numerical examples to confirm the theoretical findings. In subsection 4.1 we use Example 4.0 and Example 4.1 to verify for the 1D case optimal order convergence in $L^2$ and broken $H^1$ norms and nodal errors predicted in Theorems 2.6-2.7 using linear, quadratic, and cubic elements. For the 2D tensor case, we use Example 4.2 to verify optimal order convergence rates in Theorem 3.2. In subsection 4.2, we test our methods on a much more complicated physical example of the multi-layer porous wall model for the drug-eluting stents [27] that has been studied using IFEM [29, 30, 31, 32].

### 4.1. Numerical Verification of Theorems 2.6-2.7. Variable coefficients.

**Example 4.0.** Consider [10]

$$-(\beta u')' = f(x) = 2x, \quad u(0) = u(1) = 0$$

with the variable coefficient

$$\beta(x) = \begin{cases} x^2 + 1 & x \in [0, \alpha), \\ x^2 & x \in (\alpha, 1]. \end{cases}$$

The exact solution is

$$u(x) = \begin{cases} -x + (1-d)\tan^{-1} x & x \in [0, \alpha), \\ -x + \dfrac{d}{x} + (1-d) & x \in (\alpha, 1]. \end{cases}$$

where

$$d = \frac{(\alpha^2 \tan^{-1}\alpha - \alpha^2)(1+\alpha^2) - \gamma\alpha}{(\alpha - \alpha^2 + \alpha^2 \tan^{-1}\alpha + \gamma)(1+\alpha^2) - \gamma\alpha^2}.$$

At the interface point $\alpha$, the jump condition satisfies

$$\begin{cases} [u]_\alpha = \lambda\beta(\alpha^-)u'(\alpha^-), \\ -\beta(\alpha^-)u'(\alpha^-) = -\beta(\alpha^+)u'(\alpha^+) \end{cases} \tag{58}$$

where

$$\lambda = -\frac{(d/\alpha + (1-d)(1-\tan^{-1}\alpha))}{(d+\alpha^2)}.$$

In Table 1 and Table 2 we present the nodal errors, and scaled condition numbers (SCN), using linear, quadratic, and cubic elements for $\alpha = 1/\pi$ and $\alpha = 2/\pi$ respectively. This confirms the convergence at the nodes as predicted in Theorem 2.7 and Theorem 2.6. Figures 1 and 2 demonstrate optimal convergence rates in $L^2$ and broken $H^1$ norms for same $\alpha$ values.

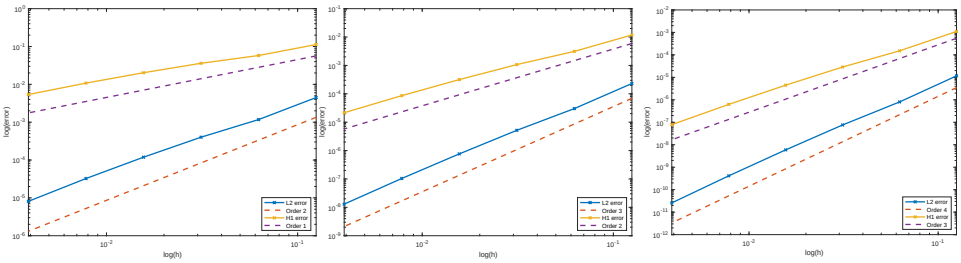

(A) Linear (B) Quadratic (C) Cubic

FIGURE 1. $L^2$ and broken $H^1$ convergence rates for Example 4.0 with $\alpha = 1/\pi$ using linear, quadratic, and cubic basis functions.

TABLE 1. Nodal errors and scaled condition numbers (SCNs) for Example 4.0 with $\alpha = 1/\pi$ using linear, quadratic, and cubic basis functions.

| Example 4.0 | Linear | | Quadratic | | Cubic | |
|---|---|---|---|---|---|---|
| | Nodal error | SCN | Nodal error | SCN | Nodal error | SCN |
| $h = 1/8$ | 1.98e-03 | 1.94e+02 | 2.13e-05 | 4.83e+03 | 2.52e-07 | 2.54e+05 |
| $h = 1/16^*$ | 4.98e-04 | 1.82e+03 | 1.50e-06 | 2.67e+05 | 4.63e-09 | 1.80e+08 |
| $h = 1/32$ | 1.41e-04 | 3.63e+03 | 1.99e-07 | 2.18e+04 | 7.84e-11 | 5.31e+08 |
| $h = 1/64$ | 5.02e-05 | 9.37e+03 | 1.81e-08 | 5.30e+04 | 1.30e-12 | 1.80e+08 |
| $h = 1/128$ | 1.49e-05 | 4.33e+04 | 1.37e-09 | 2.04e+05 | 2.07e-14 | 1.62e+09 |
| Order | $\approx 2.1$ | $\approx 1.8$ | $\approx 3.4$ | $\approx 1.3^*$ | $\approx 5.9$ | $\approx 2.5$ |

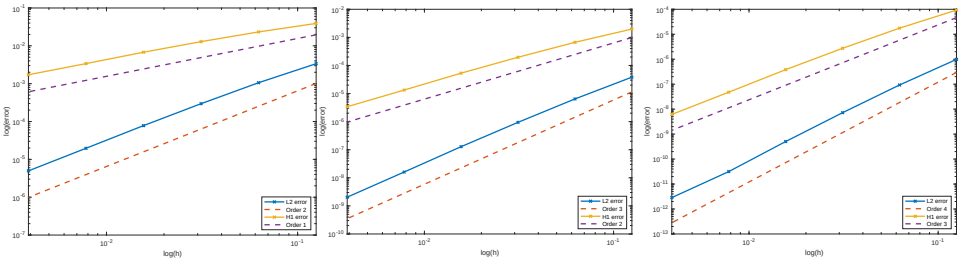

(A) Linear (B) Quadratic (C) Cubic

FIGURE 2. $L^2$ and broken $H^1$ convergence rates for Example 4.0 with $\alpha = 2/\pi$ using linear, quadratic, and cubic basis functions.

TABLE 2. Nodal errors and scaled condition numbers (SCNs) for Example 4.0 with $\alpha = 2/\pi$ using linear, quadratic, and cubic basis functions.

| Example 4.0 | Linear | | Quadratic | | Cubic | |
|---|---|---|---|---|---|---|
| | Nodal error | SCN | Nodal error | SCN | Nodal error | SCN |
| $h = 1/8^*$ | 4.54e-03 | 3.69e+03 | 1.26e-05 | 2.67e+05 | 2.87e-08 | 5.15e+08 |
| $h = 1/16$ | 1.69e-03 | 5.94e+03 | 1.46e-06 | 2.51e+04 | 4.96e-10 | 1.05e+07 |
| $h = 1/32$ | 5.62e-04 | 1.47e+04 | 1.32e-07 | 6.63e+04 | 8.16e-12 | 4.20e+07 |
| $h = 1/64$ | 1.62e-04 | 6.01e+04 | 9.89e-09 | 2.50e+05 | 1.31e-13 | 5.30e+08 |
| $h = 1/128$ | 4.07e-05 | 2.14e+05 | 6.18e-10 | 9.76e+05 | 2.10e-15 | 5.08e+09 |
| Order | $\approx 1.7$ | $\approx 1.5$ | $\approx 3.6$ | $\approx 1.8^*$ | $\approx 5.9$ | $\approx 3.0^*$ |

In general, the condition number of standard FEM depends on the mesh quality, such as element shapes and aspect ratios, polynomial orders, and material properties modelled in the differential equations. Tables 1 - 8 show the scaled condition numbers (SCNs) of the proposed enriched FEM when using linear, quadratic, and cubic elements. The main observations are: firstly, all the condition numbers roughly grow in the order of two which is the same as the standard FEM; secondly, the condition number growth of the linear element case is more robust than those of quadratic and cubic elements; thirdly, the condition numbers of quadratic or higher-order elements are more sensitive to the distance of the interface to its nearest element interface. Poorly conditioned systems result in numerical difficulties such as ill-conditioning and numerical instability. The proposed method with linear elements is robust in terms of numerical stability while the cases with higher-order elements are subject to further study and improvement.

**Example 4.1. Piecewise Constant Coefficient.** Consider

$$-(\beta u')' = f(x), \quad u(0) = u(1) = 0, \tag{59}$$

where

$$f(x) = \begin{cases} x^m & x \in [0, \alpha), \\ (x-1)^m & x \in (\alpha, 1]. \end{cases} \tag{60}$$

$m$ is a nonnegative integer. The interface point is located at $\alpha$ and

$$\beta(x) = \begin{cases} \beta^- & x \in [0, \alpha), \\ \beta^+ & x \in (\alpha, 1]. \end{cases} \tag{61}$$

The interface jump conditions are

$$[u]_\alpha = \gamma [u']_\alpha \quad \text{and} \quad [\beta u']_\alpha = 0.$$

where $\gamma = -\lambda \beta^+ \beta^- / [\beta]_\alpha$.

The exact solution is

$$u(x) = \begin{cases} \dfrac{-1}{(m+1)(m+2)\beta^-} x^{m+2} + c_1 x & x \le \alpha, \\ \dfrac{-1}{(m+1)(m+2)\beta^+} (x-1)^{m+2} + c_2 (x-1) & x \ge \alpha, \end{cases} \tag{62}$$

$$\begin{bmatrix} c_1 \\ c_2 \end{bmatrix} = \frac{1}{(\alpha - 1 - \gamma)\beta^- + (\gamma - \alpha)\beta^+} \begin{bmatrix} \alpha - \gamma - 1 & \beta^+ \\ \alpha - \gamma & \beta^- \end{bmatrix} \begin{bmatrix} R_1 \\ R_2 \end{bmatrix},$$

where

$$R_1 = \frac{\alpha^{m+1}}{m+1} - \frac{(\alpha - 1)^{m+1}}{m+1}$$

and

$$R_2 = \frac{\gamma \alpha^{m+1}}{(m+1)\beta^-} - \frac{\gamma(\alpha-1)^{m+1}}{(m+1)\beta^+} + \frac{(\alpha-1)^{m+2}}{(m+1)(m+2)\beta^+} - \frac{\alpha^{m+2}}{(m+1)(m+2)\beta^-}.$$

In the numerical experiment, we set $\lambda = 1$, $\beta^- = 100$, $\beta^+ = 1$, and $m = 6$. Tables 3 and 4 for $\alpha = 1/\pi$ and $\alpha = 2/\pi$ respectively, show that the nodal errors are exact for linear, quadratic, and cubic elements. Convergence rates for $L^2$ and broken $H^1$ errors are optimal.

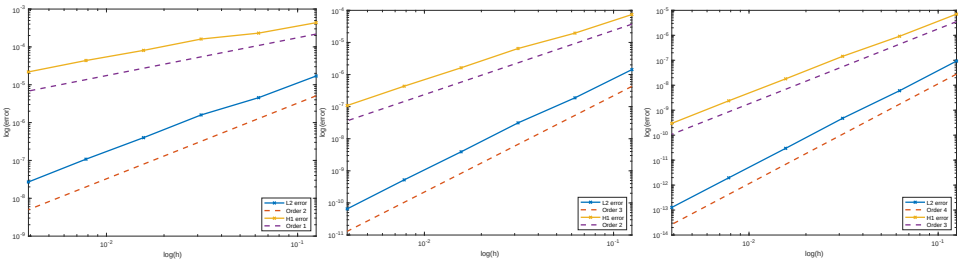

(A) Linear (B) Quadratic (C) Cubic

FIGURE 3. $L^2$ and broken $H^1$ convergence rates for Example 4.1 with $\alpha = 1/\pi$, using linear, quadratic, and cubic basis functions.

**Example 4.2.** Consider a 2D interface problem on the unit square

$$-\nabla \cdot (\beta \nabla U) = F(x, y), \text{ on } \Omega = [0, 1]^2, \quad U = 0 \text{ on } \partial\Omega, \tag{63}$$

TABLE 3. Nodal errors and scaled condition numbers (SCNs) for Example 4.1 with $\alpha = 1/\pi$, using linear, quadratic, and cubic basis functions.

| Example 4.1 | Linear | | Quadratic | | Cubic | |
|---|---|---|---|---|---|---|
| | Nodal error | SCN | Nodal error | SCN | Nodal error | SCN |
| $h = 1/8$ | 3.30e-17 | 2.15e3 | 1.06e-16 | 1.07e4 | 4.86e-17 | 4.07e4 |
| $h = 1/16$ | 2.46e-16 | 4.12e3 | 8.67e-17 | 1.54e4 | 2.47e-16 | 1.21e5 |
| $h = 1/32$ | 5.50e-16 | 8.58e3 | 1.10e-15 | 5.38e4 | 1.65e-16 | 2.51e5 |
| $h = 1/64$ | 1.45e-15 | 1.65e4 | 2.05e-16 | 6.77e4 | 2.39e-15 | 8.64e4 |
| $h = 1/128$ | 6.96e-15 | 3.43e4 | 4.99e-16 | 7.68e4 | 7.30e-15 | 1.73e5 |
| Order | - | $\approx 1.0$ | - | $\approx 0.8$ | - | $\approx 0.4$ |

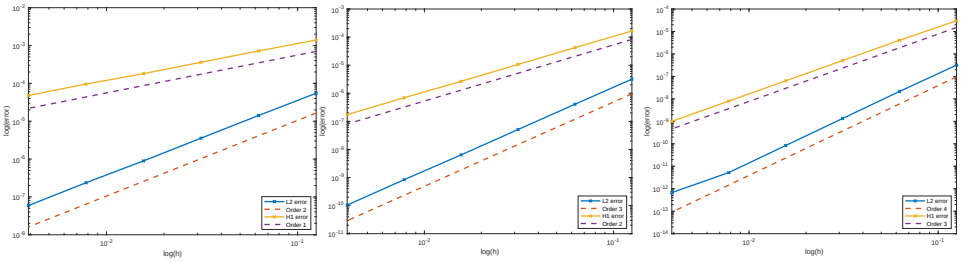

(A) Linear (B) Quadratic (C) Cubic

FIGURE 4. $L^2$ and broken $H^1$ convergence rates for Example 4.1 with $\alpha = 2/\pi$ using linear, quadratic, and cubic basis functions.

TABLE 4. Nodal errors and scaled condition numbers (SCNs) for Example 4.1 with $\alpha = 2/\pi$ using linear, quadratic, and cubic basis functions.

| Example 4.1 | Linear | | Quadratic | | Cubic | |
|---|---|---|---|---|---|---|
| | Nodal error | SCN | Nodal error | SCN | Nodal error | SCN |
| $h = 1/8^*$ | 9.19e-17 | 2.35e+04 | 3.62e-16 | 2.42e+07 | 2.79e-16 | 5.38e+10 |
| $h = 1/16$ | 6.86e-16 | 7.52e+04 | 9.54e-16 | 2.19e+06 | 8.46e-16 | 1.07e+09 |
| $h = 1/32$ | 6.74e-16 | 2.49e+05 | 3.90e-16 | 1.22e+06 | 1.23e-15 | 1.27e+07 |
| $h = 1/64$ | 8.75e-16 | 9.67e+05 | 1.48e-15 | 4.69e+06 | 2.12e-15 | 1.70e+07 |
| $h = 1/128$ | 3.76e-15 | 3.49e+06 | 1.29e-14 | 1.83e+07 | 3.50e-14 | 6.25e+07 |
| Order | - | $\approx 1.8$ | - | $\approx 1.1^*$ | - | $\approx 1.1^*$ |

with a vertical interface line $x = \alpha$ dividing $\Omega$ and the material property $\beta$ depends only on $x$:

$$\beta(x, y) = \beta(x) = \begin{cases} \beta^- & x \in [0, \alpha), \\ \beta^+ & x \in (\alpha, 1]. \end{cases} \tag{64}$$

The interface jump conditions are

$$[U]_\alpha = \gamma[\nabla U \cdot \mathbf{n}]_\alpha \quad \text{and} \quad [\beta \nabla U \cdot \mathbf{n}]_\alpha = 0$$

where $\gamma = -\lambda\beta^+\beta^+/[\beta]_\alpha$.

For this example we take $U(x, y) = u(x)Y(y)$ with $Y(y) = y(y-1)$ and

$$u(x) = \begin{cases} \beta^+ \sin \pi x & x \le \alpha \\ \beta^- \sin \pi x & x > \alpha \end{cases} \tag{65}$$

TABLE 5. Nodal errors and scaled condition numbers (SCNs) for Example 4.2 with $\alpha = 1/\pi$ using linear, quadratic, and cubic basis functions.

| Example 4.2 | Linear | | Quadratic | | Cubic | |
|---|---|---|---|---|---|---|
| | Nodal error | SCN | Nodal error | SCN | Nodal error | SCN |
| $h = 1/8$ | 6.54e-1 | 9.04e2 | 3.79e-3 | 5.98e5 | 5.78e-4 | 2.26e5 |
| $h = 1/16$ | 2.44e-1 | 2.71e4 | 3.04e-4 | 6.32e6 | 4.82e-5 | 8.10e5 |
| $h = 1/32$ | 6.10e-2 | 4.55e4 | 1.90e-5 | 7.98e5 | 3.10e-6 | 3.46e7 |
| $h = 1/64$ | 1.68e-2 | 1.92e5 | 1.26e-6 | 4.82e6 | 2.02e-7 | 2.71e8 |
| $h = 1/128$ | 4.21e-3 | 4.77e5 | 7.87e-8 | 1.32e7 | 1.24e-8 | 1.68e9 |
| Order | $\approx 1.8$ | $\approx 2.1$ | $\approx 3.9$ | $\approx 0.8$ | $\approx 3.9$ | $\approx 3.4$ |

so that the boundary conditions and the jump conditions can be easily satisfied. The right hand side function $F(x, y)$ in (63) is then defined by

$$F(x, y) = \beta^+\beta^- \sin \pi x(\pi^2 y(y-1) - 2). \tag{66}$$

Notice that $\gamma = -\frac{1}{\pi}\tan(\pi\alpha)$. In Figure 5, we demonstrate optimal $L^2$ and broken $H^1$ errors using linear, quadratic, and cubic elements, respectively. In Table 5, we list the nodal errors, and SCNs, using linear, quadratic, and cubic elements, respectively.

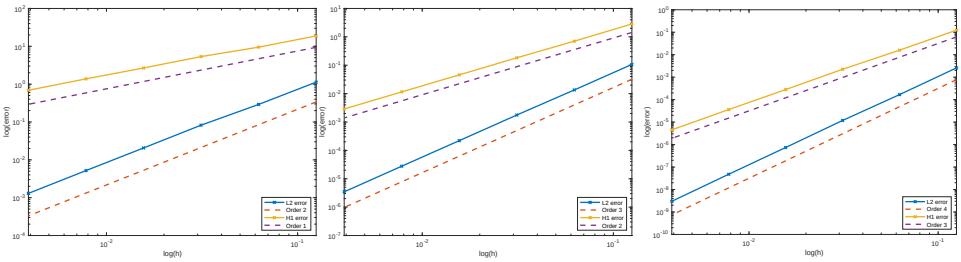

(A) Linear (B) Quadratic (C) Cubic

FIGURE 5. $L^2$ and broken $H^1$ convergence rates for Example 4.2 with $\alpha = 1/\pi$ using linear, quadratic, and cubic basis functions

**4.2. Multi-layer Porous Wall Model.** In this subsection, we test our method using the multi-layer porous wall model for the drug-eluting stents [27]. In this one-dimensional wall model of layers, a drug is released at an interface and gradually diffuses rightward. The concentration is thus discontinuous across the releasing interface and continuous in the other layers. At all interface points, a zero-flux condition is imposed. We run tests using the enriched linear, quadratic, and cubic finite element spaces. In Example 1, we place only one interface point to model the layer where the drug is delivered. In Example 2, we place two interfaces to model the layers where the concentration is continuously spread. Finally, in Example 3 we combine the previous two cases and place three interface points to simulate the full wall model. In each of the three examples, we display run results using linear, quadratic, and cubic-enriched finite elements. In all these examples, we observe that our method has optimal order convergence in the $L^2$ and broken $H^1$-norms and has comparable conditional numbers.

**Example 1. Discontinuous Solution.** Consider the two-point boundary value problem with one interface point $\alpha_0 = 1/9$

$$\frac{\partial}{\partial x}\left(-D\frac{\partial u}{\partial x} + 2\delta u\right) + \eta u = f \quad \text{in } (0,1) \tag{67}$$

subject to the the no-flux Neumann condition at $x = 0$ and the Dirichlet condition at $x = 1$:

$$D_0 u'(0) = 0, \quad u(1) = \frac{1}{3}.$$

Here the drug reaction coefficient $\eta = 0$, and the drug diffusivity $D$ and the characteristic convection parameter $\delta$ are piecewise continuous with respect to $[0, 1/9]$ and $[1/9, 1]$:

$$D(x) = \begin{cases} D_0 = 1 & x \in [0, 1/9] \\ D_1 = \frac{18(n-1)}{10n} & x \in [1/9, 1]; \end{cases}$$

$$\delta(x) = \begin{cases} \delta_0 = 0 & x \in [0, 1/9] \\ \delta = 0.5(9nD_1 - 8.1(n-1)) & x \in [1/9, 1]. \end{cases}$$

Furthermore, at the interface point $\alpha_0$, one of the jump conditions is implicit

$$\begin{cases} [u]_{\alpha_0} = \lambda D_0 u'(\alpha_0), \\ -D_0 u'(\alpha_0) = -D_1 u'(\alpha_0^+) + 2\delta_1 u(\alpha_0^+) \end{cases} \tag{68}$$

where $\lambda = 1/81(n-1)D_0$. The exact solution

$$u(x) = \begin{cases} u_0 = x^{n-1}/30, & x \in [0, 1/9], \\ u_1 = x^n/3, & x \in [1/9, 1]. \end{cases}$$

We test the effectiveness of the method with $n = 4$ and with the enrichment function in (10). The test results using linear, quadratic, and cubic elements are displayed in Table 6 and Figure 6, respectively.

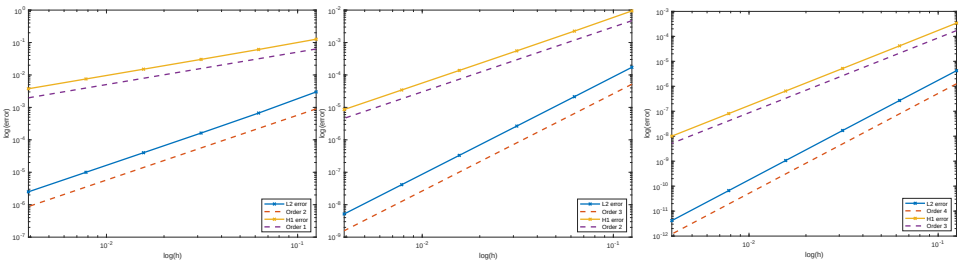

(A) Linear (B) Quadratic (C) Cubic

FIGURE 6. $L_2$ and broken $H^1$ convergence rates for Example 1 using linear, quadratic, and cubic basis functions

**Example 2. Continuous Solution.** Consider the two-point boundary value problem with two interface points $\alpha_1 = 1/3, \alpha_2 = 2/3$

$$\frac{\partial}{\partial x}\left(-D\frac{\partial u}{\partial x} + 2\delta u\right) + \eta u = f, \quad x \in (0,1) \tag{69}$$

with the boundary conditions

$$D_0 u'(0) = 0 \quad u(1) = 0.$$

TABLE 6. Nodal errors and scaled condition numbers (SCNs) for Example 1 using linear, quadratic, and cubic basis functions.

| Example 1 | Linear | | Quadratic | | Cubic | |
|---|---|---|---|---|---|---|
| | Nodal error | SCN | Nodal error | SCN | Nodal error | SCN |
| $h = 1/8$ | 1.27e-2 | 9.94e3 | 2.81e-4 | 7.57e8 | 2.37e-6 | 5.56e8 |
| $h = 1/16$ | 2.63e-3 | 4.70e8 | 1.70e-5 | 1.22e7 | 4.00e-8 | 1.35e7 |
| $h = 1/32$ | 5.86e-4 | 3.89e6 | 1.09e-6 | 4.06e6 | 6.46e-10 | 3.33e6 |
| $h = 1/64$ | 1.46e-4 | 1.03e7 | 6.75e-8 | 3.58e6 | 1.02e-11 | 5.19e6 |
| $h = 1/128$ | 3.63e-5 | 6.13e6 | 4.22e-9 | 1.29e6 | 6.94e-14 | 1.56e7 |
| Order | $\approx 2.1$ | - | $\approx 4.3$ | - | $\approx 6.2$ | - |

TABLE 7. Nodal errors and scaled condition numbers (SCNs) for Example 2 using linear, quadratic, and cubic basis functions.

| Example 2 | Linear | | Quadratic | | Cubic | |
|---|---|---|---|---|---|---|
| | Nodal error | SCN | Nodal error | SCN | Nodal error | SCN |
| $h = 1/8$ | 2.92e-2 | 1.11e3 | 1.02e-3 | 9.66e8 | 1.16e-5 | 9.80e6 |
| $h = 1/16$ | 6.43e-3 | 1.74e7 | 5.81e-5 | 1.82e7 | 1.77e-7 | 7.07e6 |
| $h = 1/32$ | 1.53e-3 | 4.78e7 | 3.72e-6 | 1.16e7 | 2.85e-9 | 1.79e7 |
| $h = 1/64$ | 3.82e-4 | 1.86e7 | 2.31e-7 | 8.15e6 | 4.49e-11 | 3.73e7 |
| $h = 1/128$ | 9.51e-5 | 3.94e7 | 1.44e-8 | 7.05e6 | 9.76e-13 | 2.90e9 |
| Order | $\approx 2.1$ | - | $\approx 4.0$ | - | $\approx 5.9$ | - |

Here with $n = 4$

$$D(x) = \begin{cases} D_1 = \frac{18(n-1)}{10n} & x \in [0, 1/3] \\ D_2 = \frac{6nD_1 - 2\delta}{3(n+1)} & x \in [1/3, 2/3] \\ D_3 = \frac{8\delta_2 - 3(n+1)D_2}{3(n+5)} & x \in [2/3, 1]; \end{cases}$$

$$\delta(x) = \begin{cases} \delta = 0.5(9nD_1 - 8.1(n-1)) & x \in [0, 1/3] \\ \delta_2 = 0.5(3(n+1)D_2 - 3nD_1 + 2\delta) & x \in [1/3, 2/3] \\ \delta_3 = 0.25(3(n-1)D_3 - 3(n+1)D_2 + 4\delta_2) & x \in [2/3, 1], \end{cases}$$

and $\eta = 10, 1, 0.1$ in respective subintervals. At the interface points $\alpha_i$ for $i = 1, 2$, the solution $u$ is continuous and

$$\begin{cases} [u]_{\alpha_i} = 0, \\ -D_i u'(\alpha_i^-) + 2\delta_i u(\alpha_i^-) = -D_{i+1} u'(\alpha_i^+) + 2\delta_{i+1} u(\alpha_i^+). \end{cases} \tag{70}$$

The exact solution is

$$u(x) = \begin{cases} u_1 = x^n/3 & x \in [0, 1/3] \\ u_2 = x^{n+1} & x \in [1/3, 2/3] \\ u_3 = 3(1-x)x^{n+1} & x \in [2/3, 1]. \end{cases}$$

The enrichment function $\psi$ is well-known [3, 12, 2]:

$$\psi(x) = \begin{cases} 0 & x \in [0, x_k] \\ \dfrac{(x_{k+1} - \alpha)(x_k - x)}{x_{k+1} - x_k} & x \in [x_k, \alpha] \\ \dfrac{(\alpha - x_k)(x - x_{k+1})}{x_{k+1} - x_k} & x \in [\alpha, x_{k+1}] \\ 0 & x \in [x_{k+1}, 1]. \end{cases} \tag{71}$$

The test results using linear, quadratic, and cubic elements are displayed in Table 7 and Figure 7, respectively.

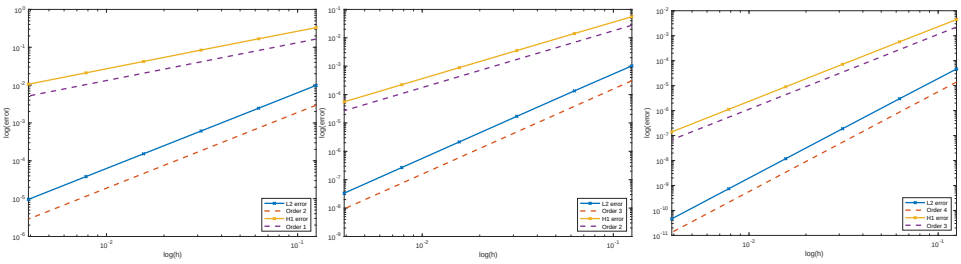

(A) Linear (B) Quadratic (C) Cubic

FIGURE 7. $L_2$ and broken $H^1$ convergence rates for example 2 using linear, quadratic, and cubic basis functions

**Example 3. Implicit and Explicit Conditions Both Present.** In this example, we combine the interfaces of the last two examples. The interface points are $\alpha_0 = 1/9$, $\alpha_1 = 1/3$ and $\alpha_2 = 2/3$. The two-point boundary value problem is

$$\frac{\partial}{\partial x}\left(-D\frac{\partial u}{\partial x} + 2\delta u\right) + \eta u = f \quad x \in (0,1) \tag{72}$$

subject to the boundary conditions

$$D_0 u'(0) = 0, \qquad u(1) = 0.$$

The coefficients are defined as follows:

$$D(x) = \begin{cases} D_0 = 1 & x \in [0, 1/9] \\ D_1 = \frac{18(n-1)}{10n}, & x \in [1/9, 1/3] \\ D_2 = \frac{6nD_1 - 2\delta}{3(n+1)} & x \in [1/3, 2/3] \\ D_3 = \frac{8\delta_2 - 3(n+1)D_2}{3(n+5)} & x \in [2/3, 1]; \end{cases}$$

$$\delta(x) = \begin{cases} \delta_0 = 0 & x \in [0, 1/9] \\ \delta = 0.5(9nD_1 - 8.1(n-1)) & x \in [1/9, 1/3] \\ \delta_2 = 0.5(3(n+1)D_2 - 3nD_1 + 2\delta) & x \in [1/3, 2/3] \\ \delta_3 = 0.25(3(n-1)D_3 - 3(n+1)D_2 + 4\delta_2) & x \in [2/3, 1]; \end{cases}$$

$n = 4$ and $\eta = 0, 10, 1, 0.1$ in respective subintervals. The exact solution is

$$u(x) = \begin{cases} u_0 = x^{n-1}/30 & [0, 1/9] \\ u_1 = x^n/3 & [1/9, 1/3] \\ u_2 = x^{n+1} & [1/3, 2/3] \\ u_3 = 3(1-x)x^{n+1} & [2/3, 1] \end{cases}$$

and it satisfies the jump condition (68) at 1/9 and (70) at the interface points 1/3 and 2/3. For the discontinuous interface point 1/9 we use the enrichment function defined in (10) and for the continuous interface points 1/3 and 2/3 we use the enrichment function in (71). The test results using linear, quadratic, and cubic elements are displayed in Table 8 and Figure 8, respectively.

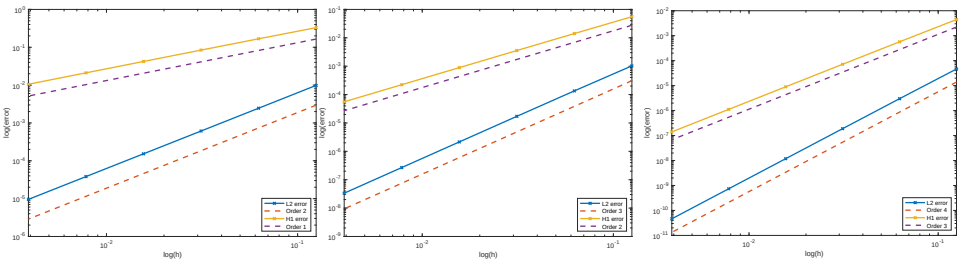

(A) Linear (B) Quadratic (C) Cubic

FIGURE 8. $L_2$ and broken $H^1$ convergence rates for Example 3 using linear, quadratic, and cubic basis functions

TABLE 8. Nodal errors and scaled condition numbers (SCNs) for Example 3 using linear, quadratic, and cubic basis functions.

| example 3 | Linear | | Quadratic | | Cubic | |
|---|---|---|---|---|---|---|
| | Nodal error | SCN | Nodal error | SCN | Nodal error | SCN |
| $h = 1/8$ | 2.92e-2 | 2.35e4 | 1.01e-3 | 4.62e8 | 1.16e-5 | 6.98e7 |
| $h = 1/16$ | 6.43e-3 | 7.18e6 | 5.81e-5 | 3.09e7 | 1.77e-7 | 1.83e7 |
| $h = 1/32$ | 1.53e-3 | 2.03e7 | 3.72e-6 | 1.04e7 | 2.85e-9 | 1.10e7 |
| $h = 1/64$ | 3.82e-4 | 2.13e7 | 2.31e-7 | 9.28e6 | 4.49e-11 | 1.59e7 |
| $h = 1/128$ | 9.51e-5 | 1.71e7 | 1.44e-8 | 4.62e6 | 9.62e-13 | 8.99e7 |
| Order | $\approx 2.1$ | - | $\approx 4.0$ | - | $\approx 5.9$ | - |

## 5. Concluding Remarks.

In this paper, we extend the lower-order GFEM developed recently for interface problems with discontinuous solutions to arbitrarily high-order elements in the spatial dimension. The main challenge has been the fact that the enrichment function constructed for linear GFEM is not sufficient to capture the discontinuous feature of the solution to the interface problem. Herein, we introduce two enrichment functions locally on the interval containing the interface. With these novel enrichment functions, we generalize the method to high-order elements. These two enrichment functions, however, introduce linear dependence among the basis functions. We overcome this issue by removing, from the standard FEM space, the bubble functions that are associated with the element containing the interface. We establish optimal error estimates for arbitrary-order elements and demonstrate the performance of the method with various numerical examples.

This work serves as preliminary development of GFEM for a larger class of interface problems as it is focused on 1D and an extension to a special case of 2D problems. A natural direction of future work is the extension to multiple dimensions with general interfaces such as curved ones. The challenge lies in the construction of enrichment functions such that the enriched space has the optimal approximability while keeping the condition number from fast growth with respect to mesh size. Another future work direction is the study of the related time-dependent interface problems. Many real application interface problems are time-dependent, for example, the precipitating quasigeostrophic equations for climate modeling. Herein, the GFEM provides an alternative numerical solver of high-order accuracy, stability, and robustness.

## References


[1] H. Ammari, J. Garnier, H. Kang, M. Lim, and S. Yu, Generalized polarization tensors for shape description, Numerische Mathematik, 126 (2014), pp. 199–224.

[2] C. Attanayake and S.-H. Chou, Superconvergence and flux recovery for an enriched finite element method, International Journal of Numerical Analysis & Modeling, 18 (2021), pp. 656–673.

[3] I. Babuška and U. Banerjee, Stable generalized finite element method (SGFEM), Computer methods in applied mechanics and engineering, 201 (2012), pp. 91–111.

[4] I. Babuška, U. Banerjee, and K. Kergrene, Strongly stable generalized finite element method: Application to interface problems, Computer Methods in Applied Mechanics and Engineering, 327 (2017), pp. 58–92.

[5] I. Babuška, U. Banerjee, and J. E. Osborn, Generalized finite element methodsmain ideas, results and perspective, International Journal of Computational Methods, 1 (2004), pp. 67–103.

[6] T. Belytschko and L. Black, Elastic crack growth in finite elements with minimal remeshing, International Journal for Numerical Methods in Engineering, 45 (1999), pp. 601–620.

[7] S. P. Bordas, E. Burman, M. G. Larson, and M. A. Olshanskii, Geometrically unfitted finite element methods and applications, Lecture Notes in Computational Science and Engineering, 121 (2017), pp. 6–8.

[8] W. Cao, X. Zhang, and Z. Zhang, Superconvergence of immersed finite element methods for interface problems, Advances in Computational Mathematics, 43 (2017), pp. 795–821.

[9] W. Cao, X. Zhang, Z. Zhang, and Q. Zou, Superconvergence of immersed finite volume methods for one-dimensional interface problems, Journal of Scientific Computing, 73 (2017), pp. 543–565.

[10] S.-H. Chou, An immersed linear finite element method with interface flux capturing recovery, Discrete & Continuous Dynamical Systems-B, 17 (2012), p. 2343.

[11] S.-H. Chou and C. Attanayake, Construction of discontinuous enrichment functions for enriched or generalized fems for interface elliptic problems in 1d, Journal of Computational and Applied Mathematics, (2023), p. 115180.

[12] Q. Deng and V. Calo, Higher order stable generalized finite element method for the elliptic eigenvalue and source problems with an interface in 1D, Journal of Computational and Applied Mathematics, 368 (2020), p. 112558.

[13] T.-P. Fries and T. Belytschko, The extended/generalized finite element method: an overview of the method and its applications, International Journal for Numerical Methods in Engineering, 84 (2010), pp. 253–304.

[14] R. Guo and T. Lin, A group of immersed finite-element spaces for elliptic interface problems, IMA Journal of Numerical Analysis, 39 (2019), pp. 482–511.

[15] R. Guo, T. Lin, and X. Zhang, Nonconforming immersed finite element spaces for elliptic interface problems, Computers & Mathematics with Applications, 75 (2018), pp. 2002–2016.

[16] D. W. Hahn and M. N. Özisik, Heat conduction, John Wiley & Sons, 2012.

[17] X. He, T. Lin, Y. Lin, and X. Zhang, Immersed finite element methods for parabolic equations with moving interface, Numerical Methods for Partial Differential Equations, 29 (2013), pp. 619–646.

[18] G. Jo and D. Y. Kwak, Recent development of immersed FEM for elliptic and elastic interface problems, Journal of the Korean Society for Industrial and Applied Mathematics, 23 (2019), pp. 65–92.

[19] J. Kačur and R. Van Keer, A nondestructive evaluation method for concrete viods: frequency differential electrical impedance scanning, SIAM Journal on Applied Mathematics, 69 (2009), pp. 1759–1771.

[20] K. Kergrene, I. Babuška, and U. Banerjee, Stable generalized finite element method and associated iterative schemes; application to interface problems, Computer Methods in Applied Mechanics and Engineering, 305 (2016), pp. 1–36.

[21] P. A. Krutitskii, The jump problem for the Helmholtz equation and singularities at the edges, Applied Mathematics Letters, 13 (2000), pp. 71–76.

[22] Z. Li, The immersed interface method using a finite element formulation, Applied Numerical Mathematics, 27 (1998), pp. 253–267.

[23] Z. Li and K. Ito, The immersed interface method: numerical solutions of PDEs involving interfaces and irregular domains, SIAM, 2006.

[24] Z. Li, T. Lin, Y. Lin, and R. C. Rogers, An immersed finite element space and its approximation capability, Numerical Methods for Partial Differential Equations: An International Journal, 20 (2004), pp. 338–367.
[25] Z. Li, T. Lin, and X. Wu, New cartesian grid methods for interface problems using the finite element formulation, Numerische Mathematik, 96 (2003), pp. 61–98.
[26] N. Moës, J. Dolbow, and T. Belytschko, A finite element method for crack growth without remeshing, International journal for numerical methods in engineering, 46 (1999), pp. 131–150.
[27] G. Pontrelli and F. de Monte, A multi-layer wall model for coronary drug-eluting stents, Int. J. Heat Mass Transf., 50 (2007), pp. 3658–3889.
[28] L. Wahlbin, Superconvergence in Galerkin finite element methods, Springer, 2006.
[29] H. Wang, J. Chen, P. Sun, and F. Qin, A conforming enriched finite element method for elliptic interface problems, Applied Numerical Mathematics, 127 (2018), pp. 1–17.
[30] H. Zhang, X. Feng, and K. Wang, Long time error estimates of IFE methods for the unsteady multi-layer porous wall model, Applied Numerical Mathematics, 156 (2020), pp. 303–321.
[31] H. Zhang, T. Lin, and Y. Lin, Linear and quadratic immersed finite element methods for the multi-layer porous wall model for coronary drug-eluting stents, International Journal of Numerical Analysis & Modeling, 15 (2018).
[32] H. Zhang and K. Wang, Long-time stability and asymptotic analysis of the IFE method for the multilayer porous wall model, Numerical Methods for Partial Differential Equations, 34 (2018), pp. 419–441.
[33] J. Zhang, Q. Deng, and X. Li, A generalized isogeometric analysis of elliptic eigenvalue and source problems with an interface, Journal of Computational and Applied Mathematics, (2021), p. 114053.
[34] Q. Zhang and I. Babuška, A stable generalized finite element method (SGFEM) of degree two for interface problems, Computer Methods in Applied Mechanics and Engineering, 363 (2020), p. 112889.
[35] Q. Zhang, U. Banerjee, and I. Babuška, Strongly stable generalized finite element method (SSGFEM) for a non-smooth interface problem, Computer Methods in Applied Mechanics and Engineering, 344 (2019), pp. 538–568.
[36] Q. Zhang, U. Banerjee, and I. Babuška, Strongly stable generalized finite element method (SSGFEM) for a non-smooth interface problem II: A simplified algorithm, Computer Methods in Applied Mechanics and Engineering, 363 (2020), p. 112926.

## Appendix A. Scales of Diagonal Entries

In this appendix, we examine the order of magnitude of the diagonal entries of the stiffness matrix for the linear element. We focus on the linear case $p = 1$. Let us calculate the diagonal entries of the stiffness matrix $\tilde{A}$ whose diagonal entries take the form of

$$\tilde{a}_{ii} = a(\xi_i, \xi_i) = \int_I \beta \xi_i' \xi_i' dx + \frac{[\xi_i]_\alpha^2}{\lambda} := a_{ii} + r_{ii}$$

with

$$\{\xi_i\} := \{\phi_1, \phi_2, \ldots, \phi_{n-1}, \phi_k\psi_0, \phi_{k+1}\psi_0, \phi_k\psi_1, \phi_{k+1}\psi_1\}.$$

Note that the jump-related terms $r_{ii} = 0$ except for $r_{jj}, j = n, n+1, n+2, n+3$.

Assume the diffusion coefficient has only two values $\beta^-, \beta^+$ for the time being (to get the general result we can use $\beta_{\min} = \min_{x\in I}\{\beta^-(x), \beta^+(x)\}, \beta_{\max} = \max_{x\in I}\{\beta^-(x), \beta^+(x)\}$). Then

$$a_{ii} = \int_0^1 \beta \phi_i' \phi_i' dx = \begin{cases} \frac{2\beta^-}{h} & i = 1, \ldots, k-1 \\ \frac{\beta^-}{h} + \frac{\beta^-}{h^2}(\alpha - x_k) + \frac{\beta^+}{h^2}(x_{k+1} - \alpha) & i = k \\ \frac{\beta^+}{h} + \frac{\beta^-}{h^2}(\alpha - x_k) + \frac{\beta^+}{h^2}(x_{k+1} - \alpha) & i = k+1 \\ \frac{2\beta^+}{h}, & i = k+2, \ldots, n-1 \end{cases}$$

and thus

$$\frac{2\beta_{\min}}{h} \le a_{ii} \le \frac{2\beta_{\max}}{h}, \quad 1 \le i \le n-1.$$

Thus, there holds

$$a_{nn} = \int_{x_k}^{x_{k+1}} \beta[(\phi_k\psi_0)']^2 dx = \beta^- m_1^2 \int_{x_k}^{\alpha} (\phi_k'(x-x_k)+\phi_k)^2 dx$$
$$a_{n+1,n+1} = \int_{x_k}^{x_{k+1}} \beta[(\phi_{k+1}\psi_0)']^2 dx = \beta^- m_1^2 \int_{x_k}^{\alpha} (\phi_{k+1}'(x-x_k)+\phi_{k+1})^2 dx$$

$$a_{n+2,n+2} = \int_{x_k}^{x_{k+1}} \beta[(\phi_k\psi_1)']^2 dx = \beta^+ m_2^2 \int_{\alpha}^{x_{k+1}} (\phi_k'(x-x_{k+1})+\phi_k)^2 dx$$
$$a_{n+3,n+3} = \int_{x_k}^{x_{k+1}} \beta[(\phi_{k+1}\psi_1)']^2 dx = \beta^+ m_2^2 \int_{\alpha}^{x_{k+1}} (\phi_{k+1}'(x-x_{k+1})+\phi_{k+1})^2 dx.$$

Note that

$$\begin{aligned}
&\int_{x_k}^{\alpha} (\phi_k'(x-x_k)+\phi_k)^2 dx = h_k \int_0^{(\alpha-x_k)/h_k} (2\hat{x}-1)^2 d\hat{x} \\
&= \frac{1}{6h_k^2}\left((2(\alpha-x_k)-h_k)^3 + h_k^3\right) \\
&= \frac{1}{6h_k^2} 2(\alpha-x_k)\left((2\alpha-x_k-x_{k+1})^2 - (2\alpha-x_k-x_{k+1})h_k + h_k^2\right) \\
&\geq \frac{1}{6h_k^2} 2(\alpha-x_k)\frac{1}{2}\left((2\alpha-x_k-x_{k+1})-h_k\right)^2 \text{ by } a^2-ab+b^2 \geq \frac{1}{2}(a-b)^2 \\
&= \frac{2}{3h_k^2}(\alpha-x_k)(\alpha-x_{k+1})^2.
\end{aligned}$$

$$\int_{x_k}^{\alpha} (\phi_{k+1}'(x-x_k)+\phi_{k+1})^2 dx = \frac{4}{3h_k^2}(\alpha-x_k)^3.$$

Also, a simple calculation leads to

$$\int_{\alpha}^{x_{k+1}} (\phi_k'(x-x_{k+1})+\phi_k)^2 dx = \frac{4}{3h_k^2}(x_{k+1}-\alpha)^3$$

$$\begin{aligned}
&\int_{\alpha}^{x_{k+1}} (\phi_{k+1}'(x-x_{k+1})+\phi_{k+1})^2 dx = h_k \int_{(\alpha-x_k)/h_k}^{1} (2\hat{x}-1)^2 d\hat{x} \\
&= \frac{1}{6h_k^2}\left((-2(\alpha-x_k)+h_k)^3 + h_k^3\right) \\
&= \frac{1}{6h_k^2} 2(x_{k+1}-\alpha)\left((2\alpha-x_k-x_{k+1})^2 + (2\alpha-x_k-x_{k+1})h_k + h_k^2\right) \\
&\geq \frac{1}{6h_k^2} 2(x_{k+1}-\alpha)\frac{1}{2}\left((2\alpha-x_k-x_{k+1})+h_k\right)^2 \text{ by } a^2+ab+b^2 \geq \frac{1}{2}(a+b)^2 \\
&= \frac{2}{3h_k^2}(x_{k+1}-\alpha)(\alpha-x_k)^2.
\end{aligned}$$

Recall the jump-related terms $r_{ii} = 0$ except for $r_{jj}, j = n, n+1, n+2, n+3$ and are of the lower order compared with $a_{ii}$ in magnitude due to the order of derivative:

$$\frac{1}{\lambda} \cdot \begin{cases} [\phi_k\psi_0]_\alpha = m_1^2(\alpha-x_k)^2(\alpha-x_{k+1})^2 h_k^{-2} \\ [\phi_{k+1}\psi_0]_\alpha = m_1^2(\alpha-x_k)^2(\alpha-x_k)^2 h_k^{-2}, \end{cases}$$

and

$$\frac{1}{\lambda}\cdot\begin{cases}[\phi_k\psi_1]_\alpha = m_2^2(\alpha - x_{k+1})^2(\alpha - x_{k+1})^2 h_k^{-2}\\ [\phi_{k+1}\psi_1]_\alpha = m_2^2(\alpha - x_k)^2(\alpha - x_{k+1})^2 h_k^{-2}.\end{cases}$$

From the above estimates, it is clear that $m_1 = (\alpha - x_{k+1})/h_k, m_2 = (\alpha - x_k/h_k)$ generate a system of condition numbers with a scale comparable to the system from the standard FEM.

Department of Mathematics, Miami University, Middletown, OH 45042, USA
*E-mail*: attanac@muohio.edu

Department of Mathematics and Statistics, Bowling Green State University, Bowling Green, OH, 43403, USA
*E-mail*: chou@bgsu.edu

School of Computing, Australian National University, Canberra, ACT 2601, Australia.
*E-mail*: quanling.deng@anu.edu.au